Bioscience Reports (2022) **42** BSR20212253
https://doi.org/10.1042/BSR20212253

PORTLAND PRESS

Research Article

Development and validation of pyroptosis-related lncRNAs prediction model for bladder cancer

Thongher Lia[1], Yanxiang Shao[1], Parbatraj Regmi[2] and Xiang Li[1]

[1]Department of Urology, West China Hospital, Sichuan University, Chengdu 610041, Sichuan Province, China; [2]Department of Biliary Surgery, West China Hospital, Sichuan University, Chengdu 610041, Sichuan Province, China

Correspondence: Xiang Li (lixiang@scu.edu.cn)

Bladder cancer (BLCA) is one of the highly heterogeneous disorders accompanied by a poor prognosis. The present study aimed to construct a model based on pyroptosis-related long-stranded non-coding RNA (lncRNA) to evaluate the potential prognostic application in bladder cancer. The mRNA expression profiles of bladder cancer patients and corresponding clinical data were downloaded from the public database from The Cancer Genome Atlas (TCGA). Pyroptosis-related lncRNAs were identified by utilizing a co-expression network of pyroptosis-related genes and lncRNAs. The lncRNA was further screened by univariate Cox regression analysis. Finally, eight pyroptosis-related lncRNA markers were established using least absolute shrinkage and selection operator (Lasso) regression and multivariate Cox regression analyses. Patients were separated into high- and low-risk groups based on the performance value of the median risk score. Patients in the high-risk group had significantly poorer overall survival (OS) than those in the low-risk group ($P<0.001$). In multivariate Cox regression analysis, the risk score was an independent predictive factor of OS (HR $>$ 1, $P<0.01$). The areas under the curve (AUCs) of the 3- and 5-year OS in the receiver operating characteristic (ROC) curve were 0.742 and 0.739, respectively. In conclusion, these eight pyroptosis-related lncRNA and their markers may be potential molecular markers and therapeutic targets for bladder cancer patients.

Introduction

Bladder cancer (BLCA) is caused by malignant tumors that grow on the mucosa of the bladder and ranks tenth among systemic malignancies worldwide [1]. With the influence of factors such as aging, environmental pollution and smoking, the morbidity and mortality of bladder cancer has been increasing [2]. Bladder cancer that has not invaded to the deeper layers of the bladder wall are treated with transurethral resection of the tumor and total cystectomy is preserved for patients with tumor invasion into the muscular layer of the bladder [3]. Over the past few decades, despite improvements in surgical and non-surgical treatments for bladder cancer, bladder cancer still has a high risk of recurrence and is associated with a poor prognosis [4–6]. There are currently no effective therapeutic targets for bladder cancer in clinical medicine [7].

Non-coding RNA (ncRNA), including microRNA (miRNA), long-stranded non-coding RNA (lncRNA), and circular RNA (circRNA) play important roles in cell growth [8]. With the advancement of transcriptome analysis, the role of dysfunctional lncRNAs in cancer has attracted considerable attention [9–11]. LncRNAs are ncRNAs ranging from 200 to 100000 nucleotides in length [12]. There has been growing evidence that aberrant lncRNA expression is associated with tumor development, diagnosis, and prognosis with the development of tumors [13,14].

Pyroptosis is a programmed form of cell death caused by an inflammatory response [15]. Not only it does play an important role in infectious diseases, but is also associated with cardiovascular diseases, central nervous system diseases, and tumors [15–17]. Pyroptosis is involved in tumorigenesis, growth, and

Received: 27 September 2021
Revised: 23 December 2021
Accepted: 10 January 2022

Accepted Manuscript online: 13 January 2022
Version of Record published: 28 January 2022

Bioscience Reports (2022) **42** BSR20212253
https://doi.org/10.1042/BSR20212253

metastasis [18]. Pyroptosis, on the one hand, stalls the growth of tumor cells and exhibits anti-tumor activity [19,20]. On the other hand, an inflammatory component is produced during scorch death, which activates pro-inflammatory cytokines that provide a microenvironment for tumor cell growth and contribute to tumor growth [21]. However, the association of the expression of pyroptosis-related lncRNA with bladder tumor developments and prognosis remains to be investigated in great detail.

In the present study, we performed an analysis of lncRNA expression datasets from The Cancer Genome Atlas (TCGA) for bladder cancer and screened for pyroptosis-related lncRNAs of prognostic value. We identified eight pyroptosis-related lncRNA signatures that have the potential to predict survival prognosis in bladder cancer patients.

Materials and methods

Data source

TCGA datasets on bladder cancer and corresponding clinical characteristics of patients were downloaded from the UCSC Xane website (UCSC Xena (xenabrowser.net)) which included 414 BLCA samples and 19 normal tissues. We incorporated patients who had clinical data with a follow-up time of more than 30 days.

Curtaining data for lncRNAs and pyroptosis-related genes

Bladder cancer data were annotated by Gencode (GENCODE version GRCh38) GTF file in the present study. Normalization of RNA-seq data expression profiles was performed by using log2 transformations. The extraction of mRNA and lncRNA genes from RNA-seq data with the Perl software (version: Strawberry-Perl-5.32.1). Pyroptosis-related genes were obtained from the prior review [22,23]. The Pearson correlation was used to measure the correlation between lncRNAs and pyroptosis-related genes. Pyroptosis-related lncRNAs were determined as those with a Pearson correlation coefficient of 0.4 and a P-value of <0.001. The Pearson correlation was used to measure the correlation between lncRNAs and pyroptosis-related genes. Pyroptosis-related lncRNAs were determined as those with a Pearson correlation coefficient of 0.4 and a P-value of <0.001.

Construction of the pyroptosis-related prognostic lncRNAs

Univariate Cox regression was used to analyze the prognostic value of pyroptosis-related lncRNAs. The least absolute shrinkage and selection operator (Lasso) regression was used to incorporate the pyroptosis-related lncRNAs with P-value <0.01 in the univariate analysis. Eventually, to create a risk score, the Lasso regression results were incorporated into a multivariate Cox model. The risk signature was constructed by multiplying linear combination of the pyroptosis-related lncRNA expression levels with a regression coefficient (β) (risk score = expression level of Gene1 * β1 + expression level of Gene2 * β2 + . . . + expression level of Gene(n) * β(n)). The patients were classified into high- and low-risk groups based on the median risk score. A log-rank test was used to compare the survival differences between the two groups.

Constructing a prognostic model

The nomogram was designed to predict the patient's survival. The model's accuracy was assessed using the C- index, calibration curve, and linear regression (receiver operating characteristic, ROC) curve. To see if risk score was an independent predictor of prognosis, we utilized multivariate Cox regression analysis including clinical characteristics.

Immune infiltration analysis

CIBERSORT and ESTIMATE were used to estimate the immune cell content of each bladder cancer patient, according to the abundance of immune cells between the high- and low-risk groups. Immune-related molecules were further analyzed to obtain information on the immune infiltration of bladder cancer.

Enrichment analyses of pyroptosis-related genes

Gene set enrichement analysis (GSEA_4.1.0 version) was performed to explain the function of gene expression data enrichment. Gene ontologies (GOs) enrichment and Kyoto Encyclopedia of Genes and Genomes (KEGG) pathway analyses were performed. We have explored the functional enrichment of prognostic lncRNAs that are associated with pyroptosis-related pathways based on the high- and low-risk groups.

Statistical analysis

The Kaplan–Meier process was then used to establish survival curves, which were then compared using the Log-rank test. The prognostic implications of pyroptosis-related lncRNA features and clinicopathological data were explored

Table 1 Multivariate analysis of the pyroptosis-related lncRNAs cohort

LncRNA	Coefficient	HR	HR.95L	HR.95H	*P*-value
AC010731.2	1.113718	3.045661	1.821714	5.091936	2.16E-05
AC034229.4	−0.78417	0.456497	0.194484	1.071501	0.071652
AL450384.2	−0.35989	0.69775	0.480704	1.012796	0.058347
IPO5P1	−0.22505	0.798476	0.62583	1.01875	0.070216
LINC02446	−0.40406	0.667604	0.495533	0.899426	0.007885
MIR100HG	0.244249	1.276663	0.997228	1.634399	0.052631
PSMB8-AS1	−0.28961	0.748554	0.578261	0.968997	0.02787
TNFRSF14-AS1	−0.52243	0.593079	0.378479	0.929359	0.022629

using Cox proportional hazards regression model, Lasso regression, and proportional hazards assumption for a Cox regression model for statistical analysis, the R programming language (version 4.1) was utilized. Statistical tests were conducted in both directions, with a P-value <0.01 deemed statistical significance.

Results

Construction of a co-expression network

Throughout the TCGA-BLCA data, 14142 lncRNAs were identified. A total of 259 pyroptosis-related genes were identified, of which 33 were expressed as mRNAs in bladder cancer. To investigate pyroptosis-related lncRNAs, a pyroptosis-related gene lncRNA co-expression network was developed. Finally, 1025 pyroptosis-related lncRNAs were identified.

Identification of prognostic pyroptosis-related lncRNA signature

Based on the results of univariate Cox analysis, 119 pyroptosis-related lncRNAs showed a predictive value for bladder cancer patients ($P<0.01$, Supplementary Table S1). Through Lasso regression, the 16 pyroptosis-related lncRNAs were identified (Figure 1A,B and Supplementary Table S2). In the multivariate analysis, eight lncRNAs were found to be associated with prognostic factors in patients (Figure 1C and Table 1). Of these, two lncRNAs (MIR100HG, AC010731.2) were the poor prognostic factors for patients (Figure 2A,B) and six lncRNAs (AL450384.2, IPO5P1, AC034229.4, TNFRSF14-AS1, PSMB8-AS1, LINC02446) were the favorable prognostic factors for patients (Figure 2C–H). These eight lncRNAs were utilized as signature lncRNAs related to pyroptosis. The formula of the risk score was as follows: Risk score = (1.113718024*AC010731.2) +(0.244249497*MIR100HG) + (−0.784173266*AC034229.4) + (−0.359894228*AL450384.2) +(−0.225050249*IPO5P1) + (−0.40405957*LINC02446) + (−0.289612092*PSMB8-AS1) + (−0.5224276 *TNFRSF14-AS1).

The prognostic impact of the established signatures

We calculated risk scores for each patient in the test dataset and divided patients into low- and high-risk groups based on the median risk score. Patients in the low-risk group overall survival (OS) had significantly improved outcomes ($P<0.001$) (Figure 3). The risk score had a significant influence on the prognosis of individuals with bladder cancer according to Cox regression analysis (Figure 4).

The pyroptosis-related lncRNA signature's clinical importance

The risk score (HR = 1.239; 95% CI: 1.153–1.332; $P<0.001$) and N-stage (HR: 1.580; 95% CI: 1.231–2.027; $P<0.001$) were independent prognostic predictors in a univariate Cox regression analysis (Table 2, Figure 5A). In multivariate analysis, only the risk score (HR = 1.232; 95% CI = 1.133−1.340; $P<0.001$, Table 2, Figure 5B) was a significant prognostic predictor. Further, the area under the curve (AUC) values for areas under the ROC curve predicting 3- and 5-year survivals were 0.742 and 0.739, respectively (Figure 5C). The AUC for areas under the multivariate ROC curve predicting showed definite predictive modeling ability, mainly through risk score, T-stage, and N-stage were 0.733, 0.653, and 0.647, respectively (Figure 5D). We validated the nomograms by testing the proportional hazards assumption of the Cox regression model to the prediction ability of the assumption model (Supplementary Figure S1). There was no statistical significance for each covariable ($P>0.05$) and no statistical significance for the global test (Supplementary Table S3). For each covariate, we generated the correlations of the corresponding sets of standardized Schoenfeld residuals with time to test for independence between residuals and time (Supplementary Figure S1), the results showed that the linear relationship between residuals and time is not significant in the proportional risk

Bioscience Reports (2022) **42** BSR20212253
https://doi.org/10.1042/BSR20212253

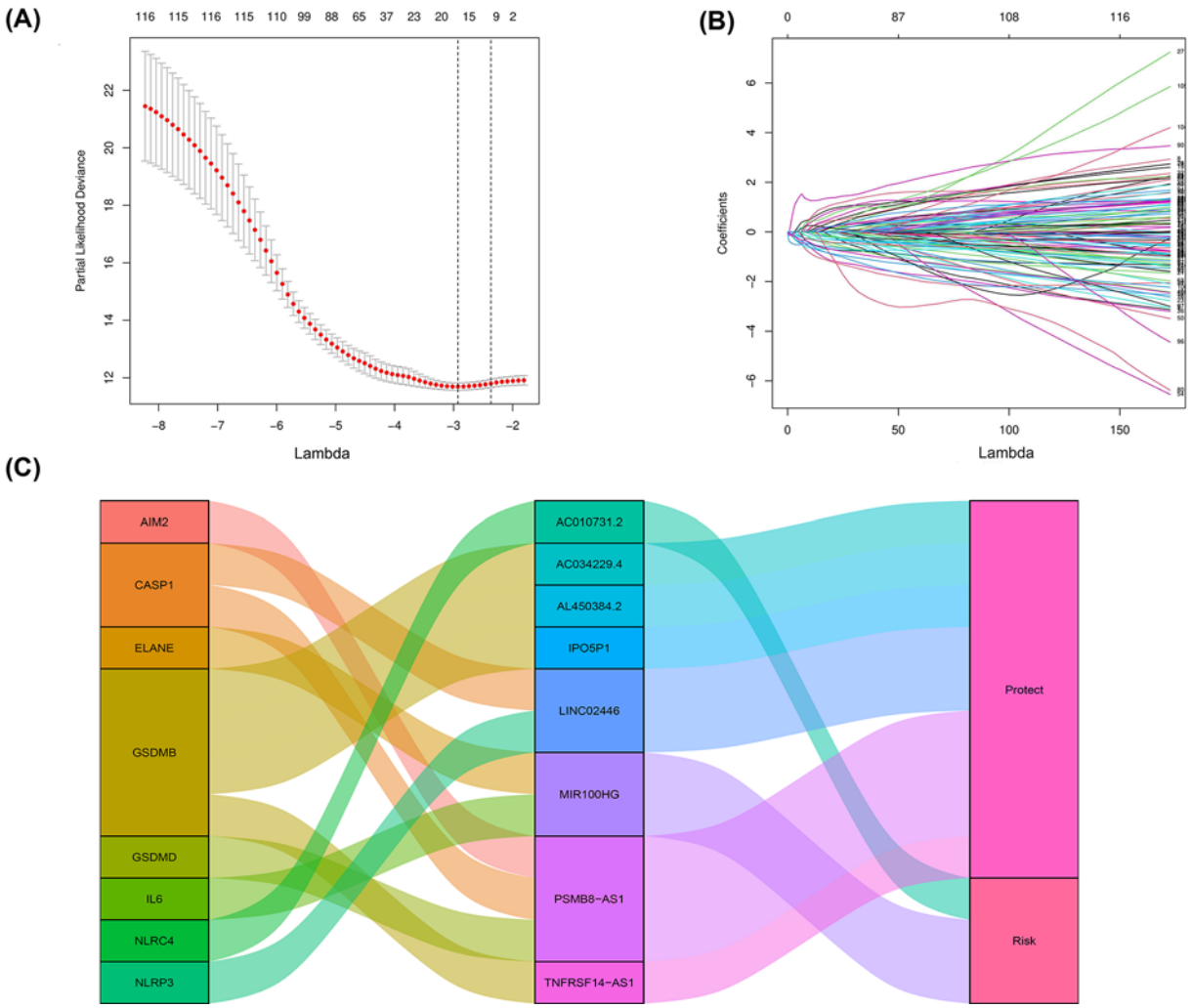

Figure 1. Identification of a 16 pyroptosis-related lncRNA risk signature for overall survival by Lasso regression analysis in TCGA cohort

(**A**) Cross-validation for tuning parameter selection in the proportional hazards model. (**B**) Lasso coefficient spectrum of 16 pyroptosis-related lncRNAs in bladder cancer. (**C**) Sankey diagram showed the association among prognostic pyroptosis-related lncRNAs, pyroptosis-related mRNAs, and risk types.

Table 2 Univariate and multivariate Cox regression analyses were used to assess the clinical features and risk scores of bladder cancer

Variable	Univariate Cox regression				Multivariate Cox regression			
	HR	HR.95L	HR.95H	*P*-value	HR	HR.95L	HR.95H	*P*-value
Age	1.022028	0.996921	1.047767	0.085988	1.018527	0.992694	1.045032	0.161348
Gender	0.621914	0.374543	1.032664	0.066397	0.600981	0.356789	1.012305	0.055621
T	1.736894	1.21213	2.488843	0.002628	1.294533	0.795159	2.107522	0.299192
N	1.579951	1.231276	2.027365	0.000324	1.099677	0.67681	1.78675	0.701219
M	2.458538	0.982327	6.153155	0.054622	1.604976	0.557005	4.624646	0.38092
Stage	1.835178	1.314974	2.561174	0.000357	1.36429	0.699753	2.659918	0.361829
Risk score	1.047395	1.028431	1.066709	6.80E-07	1.041398	1.020574	1.062647	8.28E-05

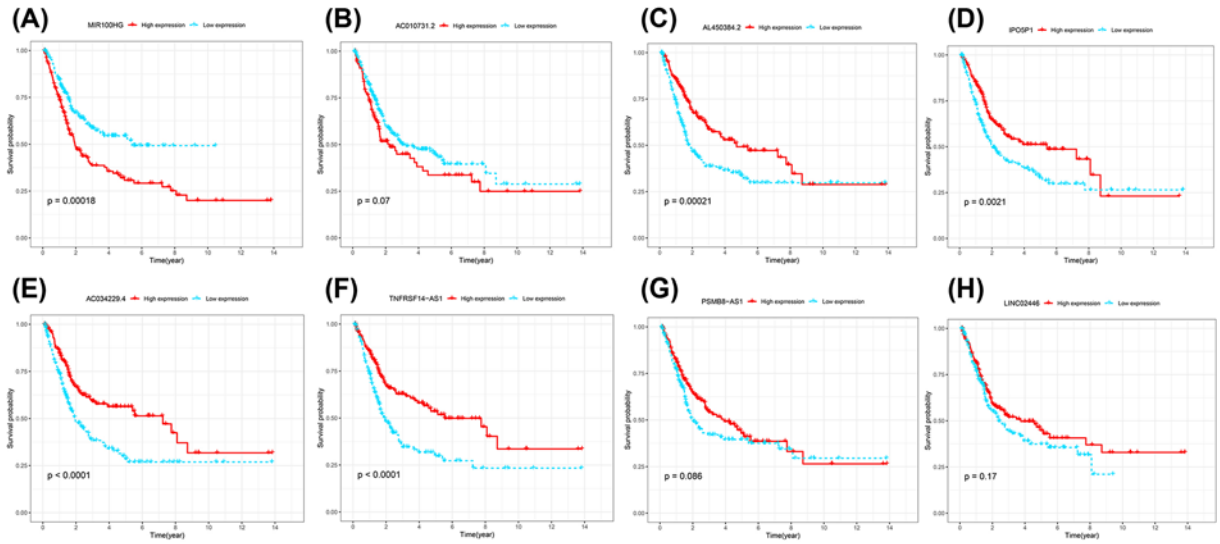

Figure 2. Kaplan–Meier survival analysis of eight pyroptosis-related lncRNAs

(**A**) MIR100HG, (**B**) AC010731.2, (**C**) AL450384.2, (**D**) IPO5P1, (**E**) AC034229.4, (**F**) TNFRSF14-AS1, (**G**) PSMB8-AS1, (**H**) LINC02446 associated with prognosis in patients with bladder cancer.

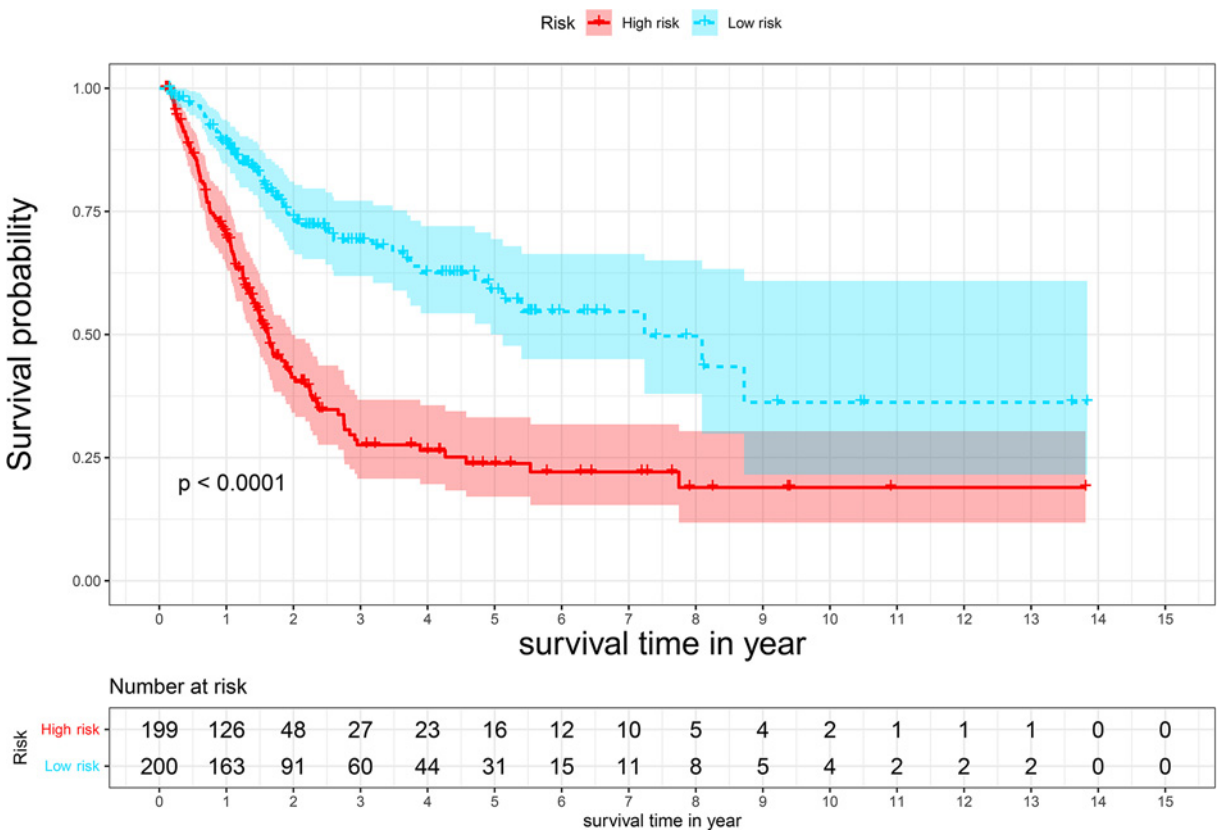

Figure 3. The risk score of Kaplan–Meier survival curves based on eight pyroptosis-related lncRNAs

hypothesis. In the Nomogram plots, we predicted the OS of bladder cancer patients at 3 and 5 years by the association of risk score and stage, as shown in (Figure 6A–C). In the prognosis model of bladder cancer, the C-index was 0.711.

Bioscience Reports (2022) **42** BSR20212253
https://doi.org/10.1042/BSR20212253

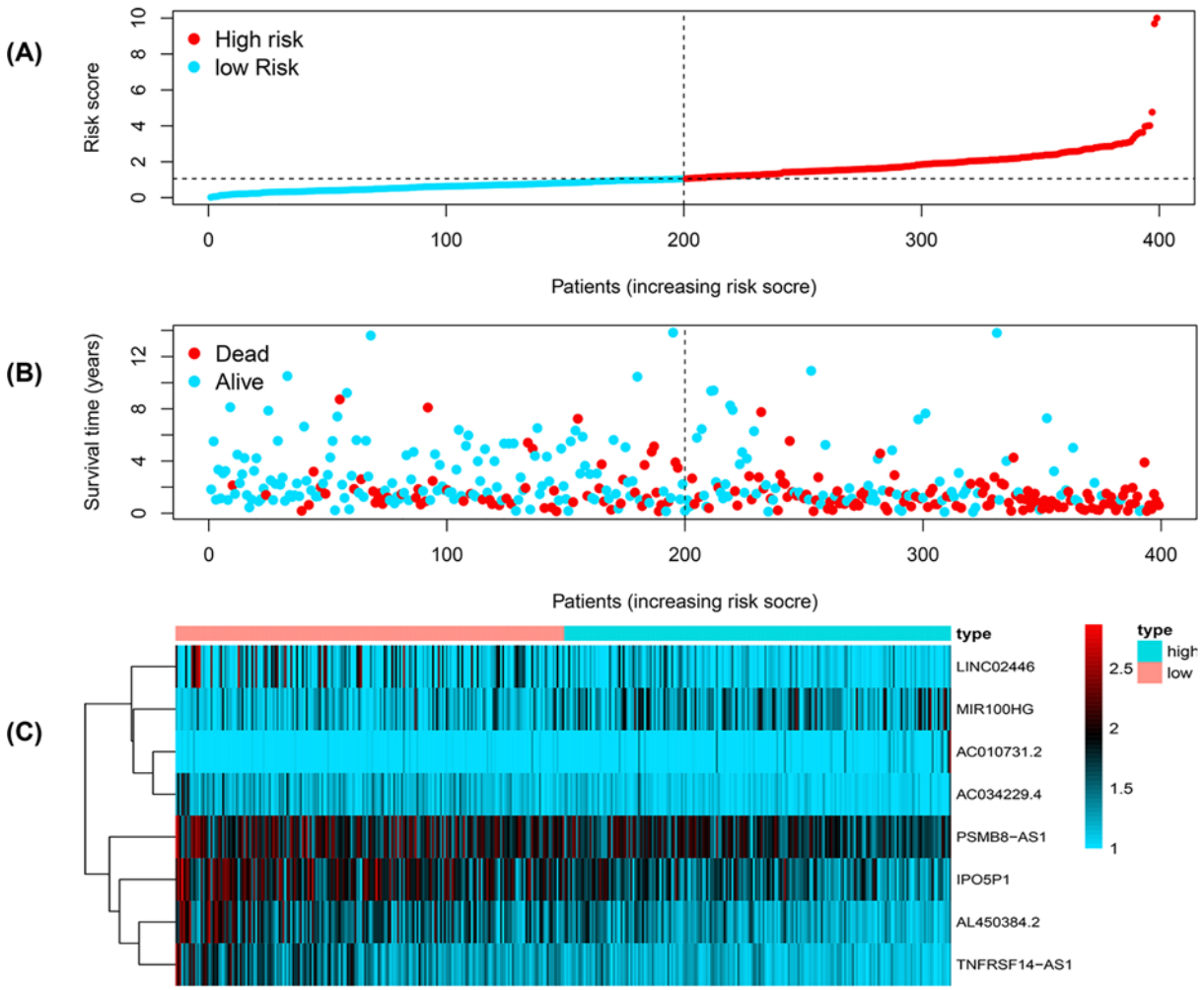

Figure 4. The analysis distribution of survival status and heat map in pyroptosis-related lncRNA signature for patients with bladder cancer

(**A**) Distribution of risk score status of bladder cancer. (**B**) The survival time of the patient. (**C**) Heat map of pyroptosis-related lncRNA expression profiles in the prognostic signature of bladder cancer.

Correlation of the expression of the eight pyroptosis-related lncRNAs with clinicopathological factors

Further, we applied whether eight pyroptosis-related associated lncRNAs are involved in the development of bladder cancer, and we investigated the relationship between the expression of eight pyroptosis-related lncRNAs and clinicopathological factors. Of the eight lncRNAs associated with pyroptosis, the results showed that AL450384.2, MIR100HG, IPO5P1, and TNFRSF14-AS1 were significantly associated with N_stage. AL450384.2, IPO5P1, LINC02446, and TNFRSF14-AS1 were significantly associated with T_stage, PSMB8-AS1 was significantly associated with M_stage, and IPO5P1 was significantly associated with gender, respectively (Supplementary Figure S2).

Relationship between pyroptosis-related lncRNAs signature and immune cells infiltration

We evaluated the infiltration of the 22 types of immune cells in the TCGA database by the CIBERSORT algorithm estimation and found that 10 types of immune cells were significantly different between the high- and low-risk groups ($P<0.05$) (Figure 7A). These included plasma cells, T cells CD8, T cells CD4 memory activated, T cells follicular helper, T cells regulatory (Tregs), Macrophages M0, Macrophages M2, Mast cells resting, Mast cells activated, and

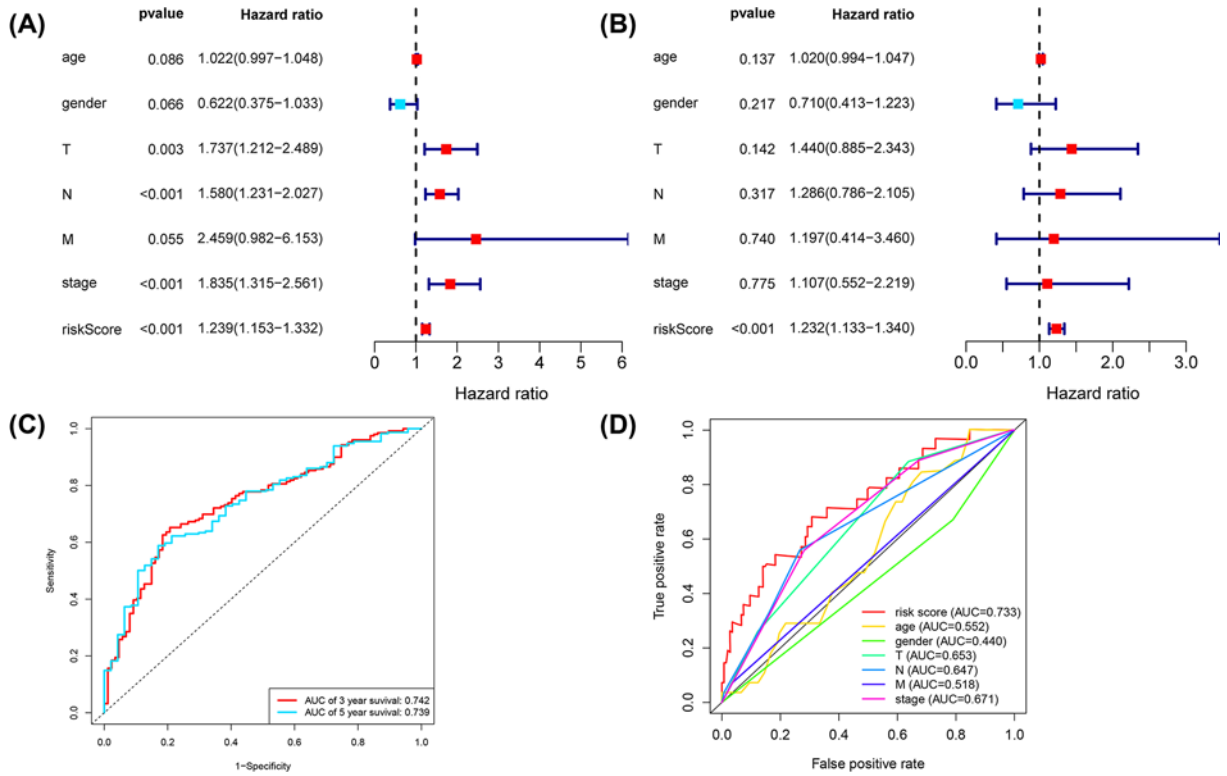

Figure 5. Univariate and multivariate Cox analyses of prognostic pyroptosis-related lncRNA risk scores for bladder cancer
(**A**) Result of univariate Cox regression. (**B**) Result of multivariate Cox regression. (**C**) ROC curve analysis shows the prognostic prediction of 3 and 5 years. (**D**) Prognostic value of composite nomogram based on several prognostic factors.

Neutrophils. Figure 7B shows the ESTIMATE scores and the differences between the low- and high-risk groups in the tumor microenvironment, stromal score, and immune score. The stromal score was significantly higher in the high-risk group ($P<0.001$), whereas the immune scores were not statistically significant in the high- and low-risk groups. Moreover, the combined ESTIMATE scores were higher in the high-risk group than in the low-risk group ($P<0.05$).

High-risk tumors show an immunosuppressive phenotype

Our results from CIBERSORT calculations revealed that macrophages were significantly up-regulated in all high-risk groups, suggesting that an immunosuppressive phenotype may exist in these tumors. Most of the chemokines (IL10, IL13, IL4 TGFB1, TGFB2, TGFB3) involved in immunosuppressive processes through macrophage induction and were also significantly up-regulated in the high-risk group ($P<0.05$) (Figure 7C). These data suggest that high-risk patients exhibit inertia in anti-tumor immunity, which could potentially contribute to their poor prognosis.

Functional analysis

We performed GO enrichment and KEGG pathways analysis of patients' samples by high-risk score. GO enrichment shows that the top ten of functions of pyroptosis-related lncRNAs in high-risk groups were mostly focused on protein transporter activity, oligosaccharide binding, monosaccharide binding, mannose-binding, disulfide oxidoreductase binding, two iron–two sulfur cluster binding, azurophil granule lumen, azurophil granule, peptidyl proline modification, chaperone-mediated protein folding (Figure 8A and Supplementary Table S4). Whereas the top ten functions of the low-risk groups were ligand-activated transcription factor activity, organism emergence from protective structure, negative regulation of cholesterol efflux, phosphatidylcholine acyl chain remodeling, branching involved in mammary gland duct morphogenesis, retinoic acid receptor signaling pathway, negative regulation of sterol transport, diacylglycerol metabolic process, histone H3K4 trimethylation, phosphatidylethanolamine acyl chain remodeling (Figure 8A and Supplementary Table S5). GSEA showed the KEGG pathways analysis of pyroptosis-related lncRNAs in high-risk groups significantly enriched in the amino sugar and nucleotide sugar metabolism, autoimmune thyroid

Bioscience Reports (2022) **42** BSR20212253
https://doi.org/10.1042/BSR20212253

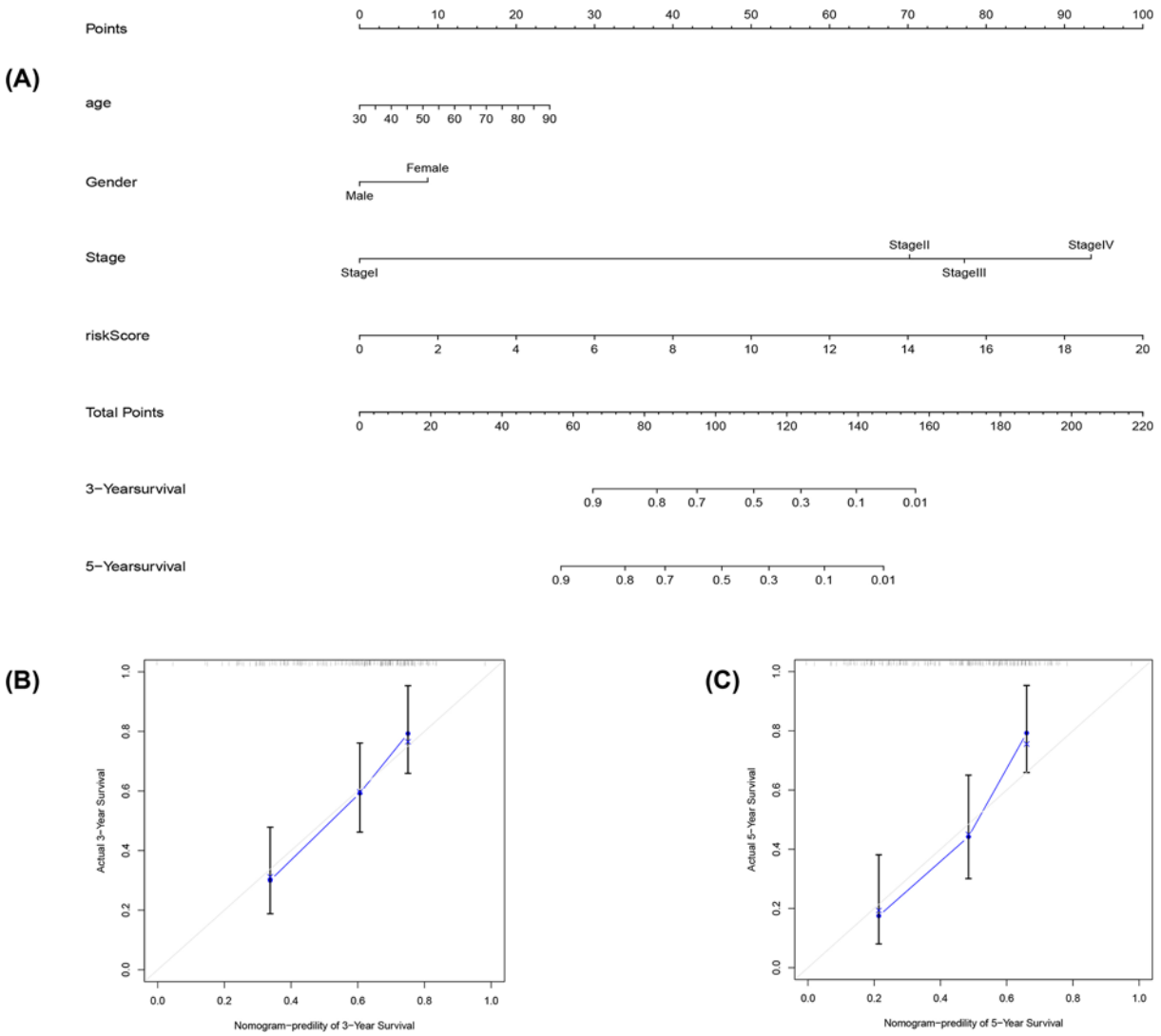

Figure 6. Prognostic model evaluation of eight pyroptosis-related associated lncRNAs

(**A**) Nomogram predicting 3- and 5-year OS based on age, gender, stage, and risk score. (**B**) Nomogram-predicted probability of 3-year survival. (**C**) Nomogram-predicted probability of 5-year survival (the 45° dotted line represents a perfect prediction, and the blue lines represent the predictive performance of the nomogram).

disease, cytokine receptor interaction, glycosaminoglycan biosynthesis chondroitin sulfate, prion diseases, proteasome, protein export, purine metabolism, renin–angiotensin system, systemic lupus erythematosus (Figure 8B and Supplementary Table S6). Interestingly, the KEGG pathway of pyroptosis-related lncRNAs in low-risk groups was mainly involved in metabolic pathways and adipocytokine signaling pathway, Notch signaling pathway, dorsoventral axis formation, primary bile acid biosynthesis (Figure 8B and Supplementary Table S7).

Discussion

At present, radical cystectomy combined with pelvic lymph node dissection and chemotherapy is the best treatment for muscle-invasive bladder cancer [3]. However, approximately 50% of patients die from metastatic disease [24], and the prognosis for patients with advanced and metastatic bladder cancer has remained unsatisfactory. Therefore, the prognostic role of molecular biomarkers is particularly important and may improve the prognosis of patients with this disorder [25]. The currently available studies showed that lncRNAs play a crucial regulatory role in

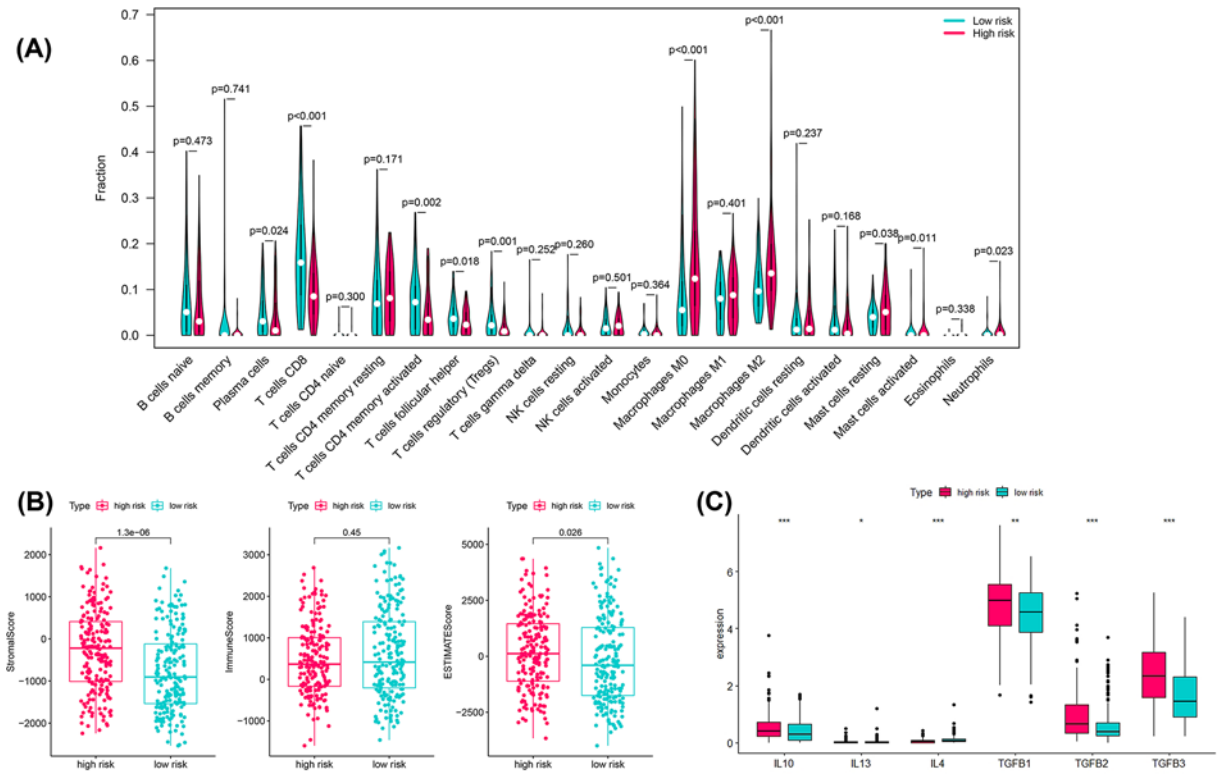

Figure 7. Immune cells infiltration analysis

(**A**) The violplots showed that 22 immune cells content in the high- and low-risk groups. **P*<0.05; ***P*<0.01; ****P*<0.001; ns, not significant. (**B**) ESTIMATE comparison of stromal, immune and tumor purity scores in high- and low-risk groups. (**C**) Expression of the immune suppressive cytokines between high- and low-risk groups. **P*<0.05, ***P*<0.01, ****P*<0.001.

pyroptosis-related biological processes in various cancer types [26]. However, there are only a few methods for predicting pyroptosis-related lncRNAs in bladder cancer patients. Our results identified eight pyroptosis-related lncRNAs, out of which two lncRNAs (AC010731.2 and MIR100HG) were associated with a poor prognosis of bladder cancer.

PSMB8-AS1 is found to have been associated with a variety of tumors. PSMB8-AS1 improves the proliferation and metastasis of PC cells by sponging miR-382-3p to up-regulate STAT1 expression. [27]. PSMB8-AS1 activated by ELK1 promotes cell proliferation in glioma via regulating miR-574-5p/RAB10 [28]. A study of epithelial–mesenchymal transition-related lncRNA signature correlating with the prognosis and progression in patients with bladder cancer suggests that PSMB8-AS1 and AC073534.1 could be used to predict the prognosis and progression of bladder cancer patients [29]. LINCOA2246 is a genomic instability-related lncRNA for bladder cancer, which may be of prognostic value and guide the clinical management of bladder cancer patients [30]. LINC02446 may influence the proliferation, migration, and invasion of bladder cancer cells. In addition, it was found to bind EIF3G protein and regulate the stability of EIF3G protein, which in turn inhibited the mTOR signaling pathway [31]. It also stimulates melanoma progression by reducing tumor-protecting miR-891a-5p and miR-203b-3p. An article on immune gene-related lncRNA found that AL450384.2 may be an important indicator of prognosis in patients with bladder cancer [32]. A recent study on the prognosis of immune gene-related lncRNAs and immunotherapy suggests that IPO5P1 may be a prognostically important value in bladder cancer patients as well as a predictor of the efficacy of immunotherapy [33]. MIR100HG plays an important role in human tumors and is an lncRNA that has received a lot of attention in the tumors, and it is expressed differently in tumor tissues dependent on the type of tumor. MIR100HG is involved in tumor proliferation, migration, and invasion in breast cancer [34], liver cancer [35], and laryngeal squamous cell carcinoma [36]. Down-regulation of MIR100HG expression in gastric cancer inhibits proliferation, migration, and invasion of gastric cancer cells [37]. It has been reported that down-regulation of MIR100HG in acute megakaryocytic leukemia may lead to inhibition of M-07e cell proliferation and induction of apoptosis and necrosis through up-regulation of TGFb expression [38]. TNFRSF14-AS1 may be a prognostically associated marker for bladder cancer immunogene-related lncRNAs [32]. For AC010731.2 and AC034229.4, the prognostic role of lncRNAs in cancer

Bioscience Reports (2022) **42** BSR20212253
https://doi.org/10.1042/BSR20212253

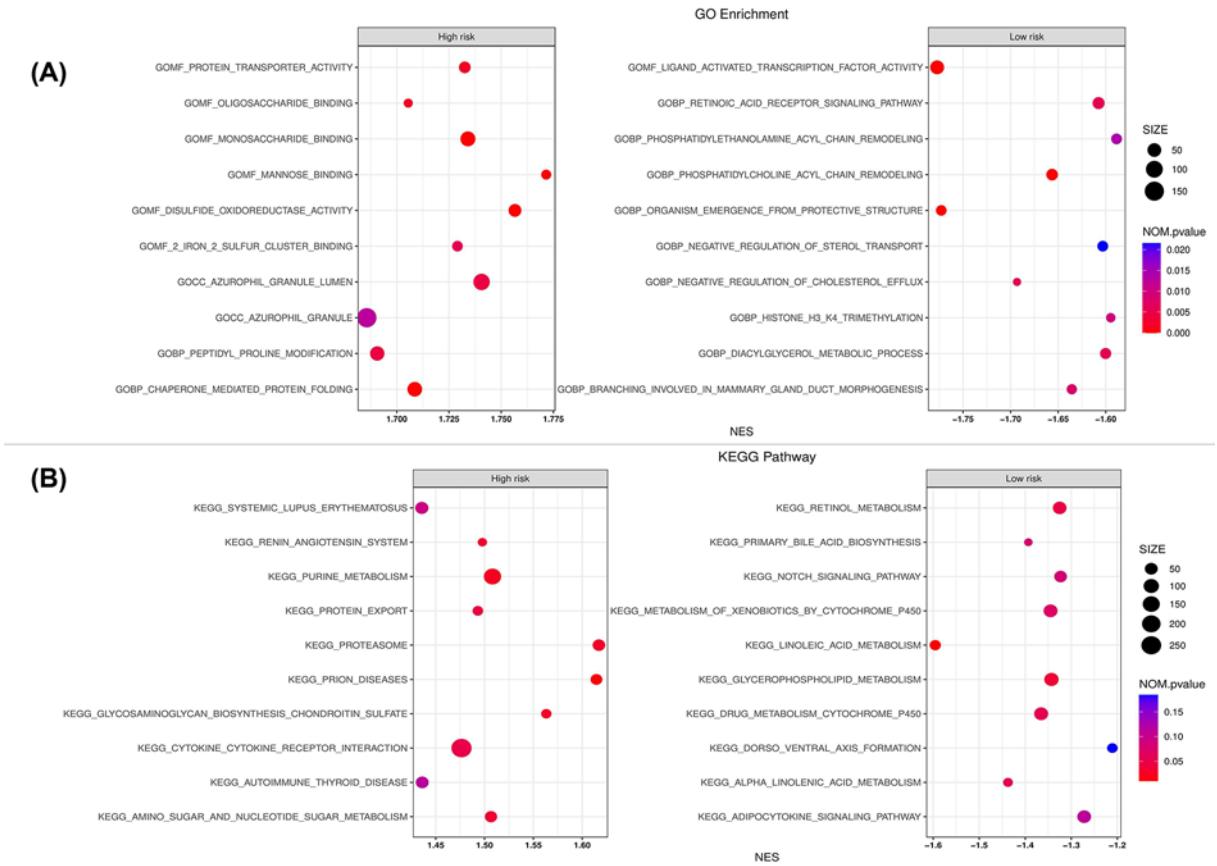

Figure 8. GO and KEGG enrichment analyses of pyroptosis-related lncRNAs

(**A**) GO enrichment analysis of top ten high-risk groups (on left) and top ten low-risk groups (on right) of pyroptosis-related lncRNAs. (**B**) Top ten KEGG pathways in high-risk groups (on left) and top ten KEGG pathways in low-risk groups (on right) of pyroptosis-related lncRNAs.

has not been reported so far. Therefore, there is a need to further research how they affect the prognosis of bladder cancer patients through their pyroptosis effects.

Immunotherapy is emerging as a new treatment option for cancer, also in uroepithelial carcinoma, where immune cell infiltration and immune checkpoints in the tumor tissue play a role in promoting or inhibiting cancer cell proliferation, invasion, and migration [39,40]. To investigate the association between scorched lncRNA signaling and immune cell infiltration, we compared the contents of immune cell content groups with different risk scores and found that Macrophages M0, Macrophages M2, Mast cells resting, Mast cells activated, Neutrophils were significantly higher than those in the low-risk group, while Plasma cells, T cells CD8, T cells CD4 memory activated, T cells follicular helper, Tregs were higher in the low-risk group than in the high-risk group. Macrophages play an important role in tumor progression [41], and these macrophages, also known as tumor-associated macrophages (TAMs), can promote tumor cell growth through a variety of mechanisms, including enhanced angiogenesis, chemoresistance, and suppression of antitumor immunity [42]. Macrophages M2 ay primarily promote tumor cell genesis and metastasis, inhibit T cell-mediated antitumor immune responses, promote tumor angiogenesis, and lead to tumor progression [43]. In the development of tumors multiple stimuli, such as anti-tumor antibodies, hypoxia, cytokines and chemokines, can activate mast cells and their mediators in the tumor microenvironment, causing them to play important immunomodulatory roles in tumor promotion and anti-tumorigenesis [44]. There is growing research evidence that tumor-infiltrating neutrophils play an important role in tumor promotion, progression, and treatment resistance [45,46]. A study of tumor-infiltrating neutrophils predicting the benefit of adjuvant chemotherapy in patients with muscle-infiltrating bladder cancer suggests that tumor-infiltrating neutrophils can be an independent prognostic factor. High tumor-infiltrating neutrophils are associated with immunosuppression in MIBC environments [47]. Most interesting are the findings that Tregs significantly infiltrate the tumor microenvironment in patients with low-risk

scores. The potential relationship between pyroptosis-related and Tregs in bladder cancer is unclear. In this study, we used the CIBERSOR calculation to infer immune cell infiltration in bladder cancer, and TAMs were up-regulated in the high-risk group. We further confirmed that cytokines involved in the immunosuppressive process (IL-4, IL-10, IL-13, TGF-β) were up-regulated in the high-risk group. Our findings show the great potential of our markers in predicting bladder cancer, which may be beneficial for immunotherapy targets in bladder malignancy.

Our study of eight markers of lncRNAs associated with pyroptosis-related significantly predicted the prognosis of bladder cancer patients. OS was longer in the low-risk group than in the high-risk group. Three- and five-year survival corresponded to an area under the ROC curve of 0.773 and 0.767, respectively. Our findings indicated that the risk score feature may help predict survival and thus may be considered as an important prognostic predictor. The model showed modest predictive performance and dependability, according to the findings of the C-index, ROC curve, and Calibration curve. The eight lncRNAs associated with pyroptosis-related were significantly correlated with stage and gender, suggesting that the eight lncRNAs associated with pyroptosis-related may vary in the extent of bladder cancer, which could help doctors plan treatment accordingly and understand the prognosis and outcome of the disease.

However, our study has some limitations. We applied public databases to construct prognostic risk models for eight pyroptosis-related lncRNA through R language and statistical analysis. While these methods have already been applied and proven in many studies, to demonstrate the eight lncRNA associated with pyroptosis-related we need to conduct an in-depth study, which includes their function and molecular mechanisms.

Conclusion

In summary, we have developed a prediction model based on eight pyroptosis-related lncRNAs (AC010731.2, MIR100HG, AC034229.4, AL450384.2, IPO5P1, LINC02446, PSMB8-AS1, TNFRSF14-AS1). This model may provide a new research strategy for exploring the pathogenesis of pyroptosis-related disorders and provide an individualized prediction of the prognosis of bladder cancer. Functional assessment and bioinformatics analysis revealed significant correlations in functionally enriched phases and pathways associated mainly with metabolic signaling pathways. Further studies are required to elucidate the mechanism of action of these pyroptosis-related lncRNAs in bladder cancer.

Data Availability

All data generated or analyzed during the present study are included in the published article.

Competing Interests

The authors declare that there are no competing interests associated with the manuscript.

Funding

This work was supported by the National Natural Science Foundation of China [grant number 81672552]; the Science and Technology Foundation of Sichuan Province [grant number 2017JY0226]; and the 1.3.5 Project for Disciplines of Excellence, West China Hospital, Sichuan University [grant number ZY2016104]. The funders had no role in the design and preparation of the manuscript.

CRedit Author Contribution

Thongher Lia: Conceptualization, Data curation, Formal analysis, Validation, Investigation, Visualization, Methodology, Writing—review & editing. **Yanxiang Shao:** Conceptualization, Data curation, Methodology. **Parbatraj Regmi:** Data curation, Investigation. **Xiang Li**: Conceptualization, Writing—review & editing, Funding acquisition.

Abbreviations

AUC, area under the curve; BLCA, bladder cancer; CI , Confidence Interval; C-index , Concordance-index; GO, gene ontology; GSEA, gene set enrichement analysis; HR , Hazard Ratio; KEGG, Kyoto Encyclopedia of Genes and Genomes; Lasso, least absolute shrinkage and selection operator; lncRNA, long non-coding RNA; OS, overall survival; PC , Pancreatic Cancer; ROC, receiver operating characteristic; TAM, tumor-associated macrophage; TCGA, The Cancer Genome Atlas; Treg, T cells regulatory.

References

1 Sung, H. et al. (2021) Global Cancer Statistics 2020: GLOBOCAN estimates of incidence and mortality worldwide for 36 cancers in 185 countries. *CA Cancer J. Clin.* **71**, 209–249, https://doi.org/10.3322/caac.21660

2 He, Y.T. et al. (2018) Incidence and mortality of bladder cancer in China, 2014. *Zhonghua Zhong Liu Za Zhi* **40**, 647–652
3 Lobo, N. et al. (2017) Landmarks in the treatment of muscle-invasive bladder cancer. *Nat. Rev. Urol.* **14**, 565–574, https://doi.org/10.1038/nrurol.2017.82
4 Lenis, A.T. et al. (2020) Bladder cancer: a review. *JAMA* **324**, 1980–1991, https://doi.org/10.1001/jama.2020.17598
5 Patel, V.G., Oh, W.K. and Galsky, M.D. (2020) Treatment of muscle-invasive and advanced bladder cancer in 2020. *CA Cancer J. Clin.* **70**, 404–423, https://doi.org/10.3322/caac.21631
6 Jordan, B. and Meeks, J.J. (2019) T1 bladder cancer: current considerations for diagnosis and management. *Nat. Rev. Urol.* **16**, 23–34, https://doi.org/10.1038/s41585-018-0105-y
7 Tran, L. et al. (2021) Advances in bladder cancer biology and therapy. *Nat. Rev. Cancer* **21**, 104–121, https://doi.org/10.1038/s41568-020-00313-1
8 Uszczynska-Ratajczak, B. et al. (2018) Towards a complete map of the human long non-coding RNA transcriptome. *Nat. Rev. Genet.* **19**, 535–548, https://doi.org/10.1038/s41576-018-0017-y
9 Gibb, E.A., Brown, C.J. and Lam, W.L. (2011) The functional role of long non-coding RNA in human carcinomas. *Mol. Cancer* **10**, 38, https://doi.org/10.1186/1476-4598-10-38
10 Mitra, S.A., Mitra, A.P. and Triche, T.J. (2012) A central role for long non-coding RNA in cancer. *Front. Genet.* **3**, 17, https://doi.org/10.3389/fgene.2012.00017
11 Prensner, J.R. and Chinnaiyan, A.M. (2011) The emergence of lncRNAs in cancer biology. *Cancer Discov.* **1**, 391–407, https://doi.org/10.1158/2159-8290.CD-11-0209
12 Mercer, T.R., Dinger, M.E. and Mattick, J.S. (2009) Long non-coding RNAs: insights into functions. *Nat. Rev. Genet.* **10**, 155–159, https://doi.org/10.1038/nrg2521
13 Crea, F. et al. (2014) Identification of a long non-coding RNA as a novel biomarker and potential therapeutic target for metastatic prostate cancer. *Oncotarget* **5**, 764–774, https://doi.org/10.18632/oncotarget.1769
14 Wang, Z. et al. (2016) Downregulation of the long non-coding RNA TUSC7 promotes NSCLC cell proliferation and correlates with poor prognosis. *Am. J. Transl. Res.* **8**, 680–687
15 Gong, W., Shi, Y. and Ren, J. (2020) Research progresses of molecular mechanism of pyroptosis and its related diseases. *Immunobiology* **225**, 151884, https://doi.org/10.1016/j.imbio.2019.11.019
16 Wang, Q. et al. (2020) Pyroptosis: a pro-inflammatory type of cell death in cardiovascular disease. *Clin. Chim. Acta* **510**, 62–72, https://doi.org/10.1016/j.cca.2020.06.044
17 He, D. et al. (2020) Long non-coding RNAs and pyroptosis. *Clin. Chim. Acta* **504**, 201–208, https://doi.org/10.1016/j.cca.2019.11.035
18 Liu, Y. et al. (2021) Non-coding RNAs in necroptosis, pyroptosis and ferroptosis in cancer metastasis. *Cell Death Discov.* **7**, 210, https://doi.org/10.1038/s41420-021-00596-9
19 Wang, Q. et al. (2020) A bioorthogonal system reveals antitumour immune function of pyroptosis. *Nature* **579**, 421–426, https://doi.org/10.1038/s41586-020-2079-1
20 Yin, H. et al. (2021) Resibufogenin suppresses growth and metastasis through inducing caspase-1-dependent pyroptosis via ROS-mediated NF-κB suppression in non-small cell lung cancer. *Anat. Rec. (Hoboken)* **304**, 302–312, https://doi.org/10.1002/ar.24415
21 Shi, J., Gao, W. and Shao, F. (2017) Pyroptosis: gasdermin-mediated programmed necrotic cell death. *Trends Biochem. Sci* **42**, 245–254, https://doi.org/10.1016/j.tibs.2016.10.004
22 Ye, Y., Dai, Q. and Qi, H. (2021) A novel defined pyroptosis-related gene signature for predicting the prognosis of ovarian cancer. *Cell Death Discov.* **7**, 71, https://doi.org/10.1038/s41420-021-00451-x
23 Lin, W. et al. (2021) Identification of the pyroptosis-related prognostic gene signature and the associated regulation axis in lung adenocarcinoma. *Cell Death Discov.* **7**, 161, https://doi.org/10.1038/s41420-021-00557-2
24 Stein, J.P. et al. (2001) Radical cystectomy in the treatment of invasive bladder cancer: long-term results in 1,054 patients. *J. Clin. Oncol.* **19**, 666–675, https://doi.org/10.1200/JCO.2001.19.3.666
25 Mitra, A.P. and Cote, R.J. (2010) Molecular screening for bladder cancer: progress and potential. *Nat. Rev. Urol.* **7**, 11–20, https://doi.org/10.1038/nrurol.2009.236
26 Cai, H.J. et al. (2021) Development and validation of a ferroptosis-related lncRNAs prognosis signature in colon cancer. *Bosn. J. Basic Med. Sci.* **21**, 5, https://doi.org/10.17305/bjbms.2020.5617
27 Zhang, H. et al. (2020) LncRNA PSMB8-AS1 contributes to pancreatic cancer progression via modulating miR-382-3p/STAT1/PD-L1 axis. *J. Exp. Clin. Cancer Res.* **39**, 179, https://doi.org/10.1186/s13046-020-01687-8
28 Shen, G. et al. (2020) PSMB8-AS1 activated by ELK1 promotes cell proliferation in glioma via regulating miR-574-5p/RAB10. *Biomed. Pharmacother.* **122**, 109658, https://doi.org/10.1016/j.biopha.2019.109658
29 Tong, H. et al. (2021) An epithelial-mesenchymal transition-related long noncoding RNA signature correlates with the prognosis and progression in patients with bladder cancer. *Biosci. Rep.* **41**, BSR20203944, https://doi.org/10.1042/BSR20203944
30 Wu, H. et al. (2021) Prediction of bladder cancer outcome by identifying and validating a mutation-derived genomic instability-associated long noncoding RNA (lncRNA) signature. *Bioengineered* **12**, 1725–1738, https://doi.org/10.1080/21655979.2021.1924555
31 Zhang, X. et al. (2021) Long non-coding RNA LINC02446 suppresses the proliferation and metastasis of bladder cancer cells by binding with EIF3G and regulating the mTOR signalling pathway. *Cancer Gene Ther.* **28**, 1376–1389, https://doi.org/10.1038/s41417-020-00285-2
32 Wang, J. et al. (2021) Identification and verification of an immune-related lncRNA signature for predicting the prognosis of patients with bladder cancer. *Int. Immunopharmacol.* **90**, 107146, https://doi.org/10.1016/j.intimp.2020.107146
33 Zhang, L. et al. (2020) Identification of immune-related lncRNA signature to predict prognosis and immunotherapeutic efficiency in bladder cancer. *Front. Oncol.* **10**, 542140, https://doi.org/10.3389/fonc.2020.542140

34 Chen, F.Y. et al. (2020) Long non-coding RNA MIR100HG promotes the migration, invasion and proliferation of triple-negative breast cancer cells by targeting the miR-5590-3p/OTX1 axis. *Cancer Cell Int.* **20**, 508, https://doi.org/10.1186/s12935-020-01580-6
35 Li, F. et al. (2021) Long noncoding RNA MIR100HG knockdown attenuates hepatocellular carcinoma progression by regulating microRNA-146b-5p/chromobox 6. *Gastroenterol. Res. Pract.* **2021**, 6832518, https://doi.org/10.1155/2021/6832518
36 Huang, Y., Zhang, C. and Zhou, Y. (2019) LncRNA MIR100HG promotes cancer cell proliferation, migration and invasion in laryngeal squamous cell carcinoma through the downregulation of miR-204-5p. *Onco Targets Ther.* **12**, 2967–2973, https://doi.org/10.2147/OTT.S202528
37 Li, J. et al. (2019) MIR100HG: a credible prognostic biomarker and an oncogenic lncRNA in gastric cancer. *Biosci. Rep.* **39**, https://doi.org/10.1042/BSR20190171
38 Bagheri, P., Sharifi, M. and Ghadiri, A. (2021) Downregulation of MIR100HG induces apoptosis in human megakaryoblastic leukemia cells. *Indian J. Hematol. Blood Transfus.* **37**, 232–239, https://doi.org/10.1007/s12288-020-01324-6
39 Liu, Z. et al. (2020) Intratumoral TIGIT(+) CD8(+) T-cell infiltration determines poor prognosis and immune evasion in patients with muscle-invasive bladder cancer. *J. Immunother. Cancer* **8**, e000978, https://doi.org/10.1136/jitc-2020-000978
40 Jiang, Q. et al. (2019) CD19(+) tumor-infiltrating B-cells prime CD4(+) T-cell immunity and predict platinum-based chemotherapy efficacy in muscle-invasive bladder cancer. *Cancer Immunol. Immunother.* **68**, 45–56, https://doi.org/10.1007/s00262-018-2250-9
41 Pan, Y. et al. (2020) Tumor-associated macrophages in tumor immunity. *Front. Immunol.* **11**, 583084, https://doi.org/10.3389/fimmu.2020.583084
42 Petty, A.J. and Yang, Y. (2017) Tumor-associated macrophages: implications in cancer immunotherapy. *Immunotherapy* **9**, 289–302, https://doi.org/10.2217/imt-2016-0135
43 Choo, Y.W. et al. (2018) M1 macrophage-derived nanovesicles potentiate the anticancer efficacy of immune checkpoint inhibitors. *ACS Nano* **12**, 8977–8993, https://doi.org/10.1021/acsnano.8b02446
44 Oldford, S.A. and Marshall, J.S. (2015) Mast cells as targets for immunotherapy of solid tumors. *Mol. Immunol.* **63**, 113–124, https://doi.org/10.1016/j.molimm.2014.02.020
45 Coffelt, S.B., Wellenstein, M.D. and de Visser, K.E. (2016) Neutrophils in cancer: neutral no more. *Nat. Rev. Cancer* **16**, 431–446, https://doi.org/10.1038/nrc.2016.52
46 Fridlender, Z.G. and Albelda, S.M. (2012) Tumor-associated neutrophils: friend or foe? *Carcinogenesis* **33**, 949–955, https://doi.org/10.1093/carcin/bgs123
47 Zhou, L. et al. (2017) Tumor-infiltrating neutrophils predict benefit from adjuvant chemotherapy in patients with muscle invasive bladder cancer. *Oncoimmunology* **6**, e1293211, https://doi.org/10.1080/2162402X.2017.1293211

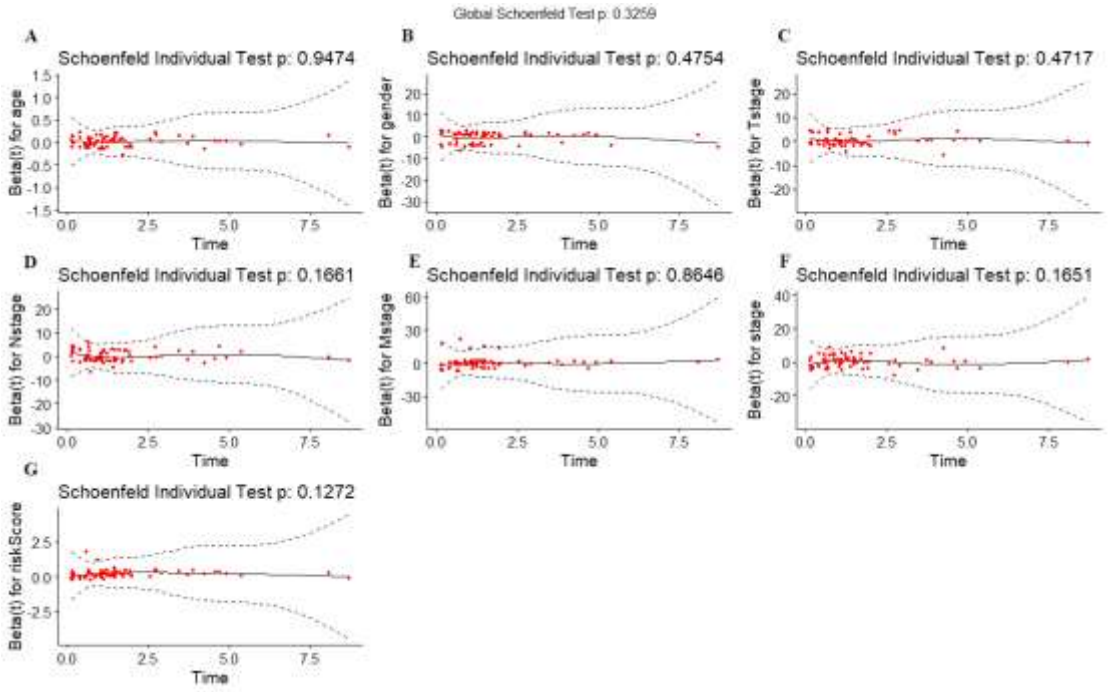

Figure S1: Correlation of each covariate generating standardized Schoenfeld residuals relative to time. (A) age, (B) gender, (C) T-stage, (D) N-stage, (E) M-stage, (F) stage, (G) risk score.

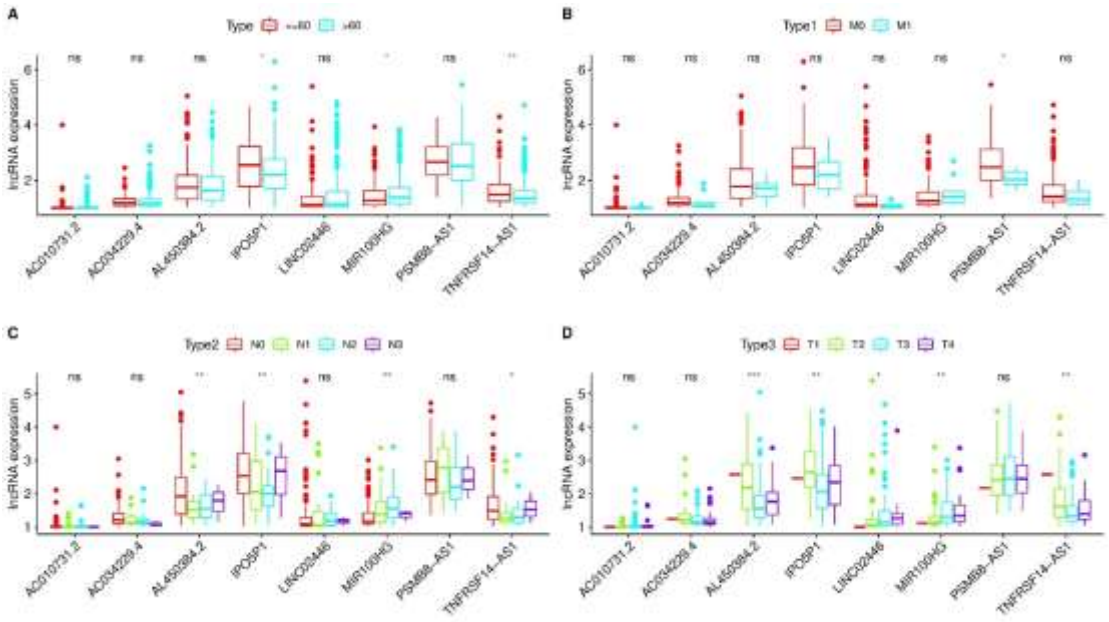

Figure S2: Expression of 8 pyroptosis-related lncRNAs and their clinical characteristics. (A) gender, (B) M-stage, (C) N-stage, (D) T-stage.

Table S1. Univariate analysis of the pyroptosis-related lncRNAs cohort

lncRNA	HR	HR.95L	HR.95H	pvalue
ZNF460-AS1	0.363784	0.186894	0.708096	0.002923
AC008760.1	0.55144	0.375899	0.808958	0.002332
AC002128.1	0.437272	0.238882	0.800426	0.007326
AC104825.1	0.613692	0.473013	0.796211	0.000237
AC009065.8	0.441701	0.279361	0.698379	0.000473
AC006042.1	0.735753	0.593684	0.91182	0.005059
AL157402.2	1.91486	1.285488	2.852372	0.001398
AC008764.6	0.358454	0.172082	0.746674	0.00614
AC018809.1	0.397489	0.228904	0.690233	0.001051
AL109811.3	0.65926	0.486379	0.893592	0.007253
AC104532.2	0.435053	0.247589	0.764455	0.003805
AC006942.1	0.490517	0.286279	0.840462	0.009526
LUCAT1	1.952342	1.34502	2.83389	0.000433
SH3BP5-AS1	0.516136	0.358874	0.742312	0.000361
AL121895.2	0.581616	0.390994	0.86517	0.007478
RPARP-AS1	0.517924	0.345613	0.776145	0.001433
AL031651.2	2.611781	1.541846	4.424179	0.000357
AC009120.2	0.449654	0.287841	0.70243	0.000445
ZNF213-AS1	0.570726	0.388196	0.839082	0.004342
AC005387.1	0.380801	0.212257	0.683179	0.001205
AL355472.1	0.65006	0.47357	0.892324	0.007702
AL139123.1	0.386823	0.195842	0.764044	0.006239
AL031714.1	0.481427	0.283341	0.817994	0.006877
RAD51-AS1	0.643774	0.463726	0.893728	0.008508
PTPRJ-AS1	1.939509	1.253545	3.000848	0.002932
AC004148.2	0.554619	0.403452	0.762424	0.000283
LYST-AS1	2.302676	1.225525	4.326565	0.009543
AL355488.1	0.63764	0.459337	0.885155	0.007168
PTOV1-AS2	0.562532	0.423576	0.747074	7.06E-05
PSMA3-AS1	0.554611	0.380273	0.808875	0.002202
SAMD12-AS1	0.39816	0.209855	0.755431	0.004828
AC009065.4	0.497734	0.314757	0.78708	0.002845
LINC01089	0.662408	0.504048	0.87052	0.00313
AC099343.2	0.401022	0.215347	0.746787	0.003972
IPO5P1	0.662639	0.547056	0.802643	2.58E-05
AC021321.1	0.193433	0.083245	0.449475	0.000134
AC010618.2	0.386414	0.194249	0.768683	0.006735
AC034229.4	0.273448	0.129061	0.57937	0.000712
LINC00115	0.361574	0.175707	0.744057	0.005729
AC011468.1	0.499466	0.353323	0.706059	8.47E-05
AL133410.1	0.355502	0.205947	0.61366	0.000205
ZKSCAN2-DT	0.481976	0.282013	0.823723	0.007605

AC005785.1	0.405465	0.221532	0.742112	0.003422
AL513477.2	0.410105	0.222627	0.755463	0.004241
AL596223.1	1.742638	1.191072	2.549627	0.004229
TMEM51-AS1	0.555595	0.392925	0.785612	0.000884
ZNF32-AS2	0.468806	0.277145	0.79301	0.004732
AL645940.1	0.426043	0.228083	0.795818	0.007443
AC005840.4	0.422997	0.269215	0.664623	0.00019
SNHG20	0.532355	0.356514	0.794924	0.002057
AC010326.3	0.635449	0.483383	0.835354	0.001158
AL162258.2	0.360162	0.188943	0.686537	0.001918
LINC01871	0.803151	0.6814	0.946656	0.008961
ETV5-AS1	2.167217	1.266142	3.709559	0.004795
AC131210.1	2.166911	1.203887	3.900286	0.009916
AC073335.2	0.610162	0.466837	0.797491	0.000299
LINC01355	0.610979	0.422849	0.88281	0.008697
STAG3L5P-PVRIG2P-PILRB	0.255515	0.13433	0.486029	3.19E-05
AC063948.1	0.508729	0.308392	0.83921	0.008136
ARHGAP27P1-BPTFP1-KPNA2P3	0.634395	0.468182	0.859616	0.003327
RBMS3-AS3	2.316836	1.518084	3.535856	9.81E-05
AL353622.1	0.445416	0.287652	0.689707	0.000289
AC011477.3	0.672853	0.513386	0.881855	0.004092
AC003102.1	0.6702	0.499335	0.899531	0.007696
AL022328.2	0.555717	0.383928	0.804373	0.001847
AC022306.2	0.461552	0.267042	0.797742	0.005617
AC089983.1	1.905992	1.198623	3.030814	0.00642
TGFB2-AS1	1.65711	1.131102	2.427731	0.009535
AL591895.1	0.744675	0.622041	0.891485	0.001322
AL022322.1	0.559295	0.406384	0.769741	0.000363
LINC02446	0.706336	0.557567	0.8948	0.003963
AC093726.2	0.40518	0.206782	0.79393	0.00848
AC034236.2	0.34261	0.189799	0.61845	0.000379
U47924.1	0.358431	0.174581	0.735891	0.005181
AL390728.6	0.591615	0.467909	0.748027	1.16E-05
USP30-AS1	0.700927	0.553726	0.88726	0.003132
AL035563.1	0.453435	0.25572	0.804015	0.006801
AC234772.2	1.605536	1.142722	2.255795	0.006354
AC068620.2	0.373497	0.181085	0.770355	0.007669
AC104971.2	2.310204	1.266398	4.214352	0.006334
AC093788.1	0.405874	0.236773	0.695745	0.001041
AC135050.3	0.389924	0.206042	0.737911	0.003806
AC010201.2	0.380137	0.182416	0.792167	0.009826
AC105177.1	2.520811	1.534613	4.140776	0.000261
AC120053.1	0.545002	0.391278	0.759122	0.000331

AC010542.5	0.551084	0.399441	0.760296	0.000285
AC025171.4	0.456601	0.255569	0.815767	0.008104
AC243830.2	0.416478	0.21736	0.798001	0.008289
AC087741.1	0.507989	0.349847	0.737617	0.000372
AC010731.2	2.733902	1.767253	4.229285	6.24E-06
MIR100HG	1.366534	1.084273	1.722275	0.00816
AC078880.5	0.324983	0.151189	0.698556	0.003992
AC084871.1	1.929952	1.227348	3.034765	0.004413
AC020663.2	0.441619	0.240812	0.809872	0.008253
AC016737.1	0.342604	0.16454	0.713368	0.004202
AF178030.1	2.018385	1.186306	3.434086	0.009597
AL355102.1	1.871683	1.230276	2.84749	0.003412
SNHG16	1.572311	1.11788	2.211474	0.009316
AL139089.1	0.44871	0.278078	0.724044	0.001028
TNFRSF14-AS1	0.374913	0.243482	0.57729	8.40E-06
AL136295.2	0.230709	0.108925	0.488655	0.000128
AC005726.3	0.623718	0.46575	0.835263	0.001535
AC027020.2	0.371091	0.217408	0.63341	0.000279
AC115989.1	1.882924	1.179253	3.006481	0.008036
AC104051.2	1.947026	1.266024	2.994343	0.002413
AC007038.2	0.538299	0.343342	0.843958	0.006947
AL354919.2	0.6465	0.512065	0.816229	0.000245
AL450384.2	0.53688	0.403538	0.714282	1.96E-05
AC078880.3	0.545008	0.371788	0.798931	0.001869
PSMB8-AS1	0.764962	0.631948	0.925973	0.005976
AC245884.8	0.52928	0.336685	0.832045	0.00584
AL021707.6	0.603261	0.464769	0.783021	0.000146
AL390719.2	0.790673	0.68751	0.909315	0.000992
AC055822.1	0.544219	0.377798	0.78395	0.001087
AC024060.1	0.569668	0.443987	0.730926	9.66E-06
AC008610.1	0.562016	0.402892	0.783987	0.000691
AC011477.2	0.653545	0.482586	0.885067	0.005977
ZNF32-AS1	0.431919	0.238102	0.783507	0.005729
AL355353.1	0.691152	0.575104	0.830616	8.19E-05

Table S2. LASSO regression coefficients of sixteen pyroptosis-related lncRNAs.

lncRNA	Coefficient
AL031651.2	0.144994
IPO5P1	-0.18597
AC021321.1	-0.43346
AC034229.4	-0.37206
AC011468.1	-0.28031
STAG3L5P-PVRIG2P-PILRB	-0.39037
RBMS3-AS3	0.259661
LINC02446	-0.44938
USP30-AS1	-0.17052
AC010731.2	1.395285
MIR100HG	0.064872
TNFRSF14-AS1	-0.51875
AL354919.2	-0.12758
AL450384.2	-0.28801
PSMB8-AS1	-0.0486
AL355353.1	-0.01124

Table S3: Proportional Hazards Assumption of nomogram Cox Regression

	chisq	df	P
age	0.00436	1	0.95
Gender	0.50937	1	0.48
T stage	0.51808	1	0.47
N stage	1.91813	1	0.17
M stage	0.02906	1	0.86
Stage	1.92675	1	0.17
Risk score	2.32676	1	0.13
GLOBAL	8.07666	7	0.33

Table S4. Gene set enrichment GO analysis results of high risk group 8 pyroptosis-related lncRNAs (Top 10 p-value)

NAME	SIZE	NES	NOM p-val	FDR q-val	LEADING EDGE
GOMF_PROTEIN_TRANSPORTER_ACTIVITY	29	1.73256	0.001908	1	tags=48%, list=12%, signal=55%
GOMF_OLIGOSACCHARIDE_BINDING	16	1.705475	0.00202	0.991089	tags=63%, list=11%, signal=70%
GOMF_MONOSACCHARIDE_BINDING	67	1.734055	0	1	tags=54%, list=13%, signal=62%
GOMF_MANNOSE_BINDING	19	1.771577	0	1	tags=68%, list=16%, signal=81%
GOMF_DISULFIDE_OXIDOREDUCTASE_ACTIVITY	40	1.756601	0	1	tags=70%, list=16%, signal=84%
GOMF_2_IRON_2_SULFUR_CLUSTER_BINDING	22	1.729062	0.005758	0.91257	tags=50%, list=10%, signal=55%
GOCC_AZUROPHIL_GRANULE_LUMEN	91	1.740597	0.004107	1	tags=63%, list=17%, signal=76%
GOCC_AZUROPHIL_GRANULE	153	1.685629	0.012474	1	tags=55%, list=15%, signal=65%
GOBP_PEPTIDYL_PROLINE_MODIFICATION	58	1.69061	0.004024	1	tags=45%, list=14%, signal=52%
GOBP_CHAPERONE_MEDIATED_PROTEIN_FOLDING	63	1.7086	0	1	tags=48%, list=11%, signal=54%

Table S5. Top 10 function of 8 pyroptosis-related lncRNAs from GO enrichment analysis results of low-risk group (Top 10 p-value)

NAME	SIZE	NES	NOM p-val	FDR q-val	LEADING EDGE
GOMF_LIGAND_ACTIVATED_TRANSCRIPTION_FACTOR_ACTIVITY	52	-1.77725	0	0.93056	tags=52%, list=14%, signal=61%
GOBP_ORGANISM_EMERGENCE_FROM_PROTECTIVE_STRUCTURE	22	-1.7729	0	0.506387	tags=59%, list=16%, signal=70%
GOBP_NEGATIVE_REGULATION_OF_CHOLESTEROL_EFFLUX	15	-1.69327	0.005952	1	tags=53%, list=16%, signal=63%
GOBP_PHOSPHATIDYLCHOLINE_ACYL_CHAIN_REMODELING	29	-1.65638	0	1	tags=45%, list=10%, signal=50%
GOBP_BRANCHING_INVOLVED_IN_MAMMARY_GLAND_DUCT_MORPHOGENESIS	20	-1.63565	0.008065	1	tags=65%, list=18%, signal=79%
GOBP_RETINOIC_ACID_RECEPTOR_SIGNALING_PATHWAY	32	-1.60752	0.005859	1	tags=50%, list=17%, signal=60%
GOBP_NEGATIVE_REGULATION_OF_STEROL_TRANSPORT	23	-1.60312	0.021526	1	tags=52%, list=16%, signal=62%
GOBP_DIACYLGLYCEROL_METABOLIC_PROCESS	25	-1.6001	0.006036	1	tags=48%, list=14%, signal=56%
GOBP_HISTONE_H3_K4_TRIMETHYLATION	17	-1.59473	0.009728	1	tags=76%, list=16%, signal=90%
GOBP_PHOSPHATIDYLETHANOLAMINE_ACYL_CHAIN_REMODELING	23	-1.58862	0.014199	1	tags=43%, list=10%, signal=48%

Table S6. KEGG pathway analysis results 8 pyroptosis-related lncRNAs in high-risk group (Top 10 p-value).

NAME	SIZE	NES	NOM.pvalue	FDR	LEADING EDGE
KEGG_PROTEASOME	46	1.6171805	0.028056113	0.8888676	tags=76%, list=13%, signal=88%
KEGG_PRION_DISEASES	35	1.6146219	0.011976048	0.45655707	tags=54%, list=16%, signal=65%
KEGG_GLYCOSAMINOGLYCAN_BIOSYNTHESIS_CHONDROITIN_SULFATE	22	1.5632548	0.029239766	0.5445688	tags=64%, list=16%, signal=75%
KEGG_PURINE_METABOLISM	156	1.5081213	0.022633744	0.7085648	tags=55%, list=24%, signal=72%
KEGG_AMINO_SUGAR_AND_NUCLEOTIDE_SUGAR_METABOLISM	42	1.5065918	0.036144577	0.5736164	tags=50%, list=16%, signal=59%
KEGG_RENIN_ANGIOTENSIN_SYSTEM	17	1.4977536	0.03426124	0.5124177	tags=59%, list=15%, signal=69%
KEGG_PROTEIN_EXPORT	24	1.4931266	0.042944785	0.45845512	tags=54%, list=17%, signal=65%
KEGG_CYTOKINE_CYTOKINE_RECEPTOR_INTERACTION	264	1.476344	0.049603175	0.4640261	tags=45%, list=15%, signal=53%
KEGG_AUTOIMMUNE_THYROID_DISEASE	50	1.4361321	0.114173226	0.57255715	tags=40%, list=10%, signal=45%
KEGG_SYSTEMIC_LUPUS_ERYTHEMATOSUS	55	1.4357249	0.09325397	0.51699173	tags=65%, list=18%, signal=80%

Table S7. KEGG pathway analysis results 8 pyroptosis-related lncRNAs in low-risk group (Top 10 p-value).

NAME	SIZE	NES	NOM.pvalue	FDR	LEADING EDGE
KEGG_LINOLEIC_ACID_METABOLISM	29	-1.59555	0.00996	0.558545	tags=48%, list=13%, signal=55%
KEGG_ALPHA_LINOLENIC_ACID_METABOLISM	19	-1.43757	0.053254	1	tags=53%, list=12%, signal=60%
KEGG_PRIMARY_BILE_ACID_BIOSYNTHESIS	16	-1.3933	0.079612	1	tags=38%, list=5%, signal=40%
KEGG_DRUG_METABOLISM_CYTOCHROME_P450	71	-1.36543	0.054264	1	tags=41%, list=15%, signal=48%
KEGG_METABOLISM_OF_XENOBIOTICS_BY_CYTOCHROME_P450	69	-1.34506	0.068762	0.90958	tags=41%, list=15%, signal=48%
KEGG_GLYCEROPHOSPHOLIPID_METABOLISM	77	-1.34308	0.035573	0.767071	tags=34%, list=15%, signal=40%
KEGG_RETINOL_METABOLISM	64	-1.32524	0.048544	0.732856	tags=38%, list=13%, signal=43%
KEGG_NOTCH_SIGNALING_PATHWAY	47	-1.32319	0.084314	0.649976	tags=64%, list=25%, signal=85%
KEGG_ADIPOCYTOKINE_SIGNALING_PATHWAY	67	-1.27198	0.109756	0.783415	tags=46%, list=18%, signal=56%
KEGG_DORSO_VENTRAL_AXIS_FORMATION	24	-1.21072	0.184	0.966428	tags=42%, list=14%, signal=48%